

# Efficient High Order Matching

Michael Chertok and Yosi Keller

**Abstract**—We present a computational approach to high-order matching of data sets in  $\mathbb{R}^d$ . Those are matchings based on data affinity measures that score the matching of more than two pairs of points at a time. High-order affinities are represented by tensors and the matching is then given by a rank-one approximation of the affinity tensor and a corresponding discretization. Our approach is rigorously justified by extending Zass and Shashua's hypergraph matching [40] to high-order spectral matching. This paves the way for a computationally efficient dual-marginalization spectral matching scheme. We also show that, based on the spectral properties of random matrices, affinity tensors can be randomly sparsified while retaining the matching accuracy. Our contributions are experimentally validated by applying them to synthetic as well as real data sets.

**Index Terms**—High-order assignment, probabilistic matching, spectral relaxation.

## 1 INTRODUCTION

GRAPH matching is a fundamental problem in theoretical computer science and relates to a gamut of research topics in computer vision and machine learning. Those include the registration of sets of points in  $\mathbb{R}^d$  [22], [38], object recognition [6], shape retrieval [12], and symmetry analysis [16], to name a few. Given a set of points, graph nodes can represent the points and the graph edges encode their distances. Hence, computing graph correspondence paves the way for recovering point correspondences.

Over the years, a myriad of point matching approaches have been suggested. These can be categorized as those that solve the linear assignment problem (bipartite graph matching) versus those that solve high order assignment (HOA) problems. Given two sets of points in  $\mathbb{R}^d$  such that  $S_1 = \{\mathbf{x}_i\}_{i=1}^{n_1}$  and  $S_2 = \{\mathbf{y}_j\}_{j=1}^{n_2}$ , the assignment problem is to find the set of assignments

$$C \triangleq \{c_i\}_{i=1}^{n_1} = \{\mathbf{x}_i, \mathbf{y}_{i'}\}_{i=1}^{n_1}. \quad (1)$$

Without loss of generality, it is common to add a dummy element  $\mathbf{y}_0$  to the set  $S_2$  such that  $\{\mathbf{x}_i, \mathbf{y}_0\}$  implies that  $\mathbf{x}_i$  is not matched to any point in  $S_2$ . We represent the correspondence by an indicator vector  $\mathbf{z} \in \{0, 1\}^{n_1 n_2}$ , which is the rowwise vectorized replica of the assignment matrix  $Z \in \{0, 1\}^{n_1 \times n_2}$ , where  $Z_{ii'} = 1$  implies that  $\mathbf{x}_i$  corresponds to  $\mathbf{y}_{i'}$  and  $Z_{ii'} = 0 \forall i'$  implies that  $\mathbf{x}_i$  is not matched to any point in  $S_2$ .

The matching is defined by an affinity matrix  $A$  such that

$$A_{i,i'} = \Omega_1(\mathbf{x}_i, \mathbf{y}_{i'}) = \Omega_1(c_i)$$

is the affinity of matching  $\mathbf{x}_i$  to  $\mathbf{y}_{i'}$  and  $\Omega_1$  is the linear assignment affinity measure. The optimal assignment is thus given by

- The authors are with the School of Engineering, Bar-Ilan University, Ramat Gan, Israel. E-mail: {michael.chertok, yosi.keller}@gmail.com.

Manuscript received 1 Nov. 2009; revised 12 Jan. 2010; accepted 12 Jan. 2010; published online 25 Feb. 2010.

Recommended for acceptance by P. Felzenszwalb.

For information on obtaining reprints of this article, please send e-mail to: tpami@computer.org, and reference IEEECS Log Number TPAMI-2009-11-0735.

Digital Object Identifier no. 10.1109/TPAMI.2010.51.

$$\begin{aligned} \mathbf{z}^* &= \arg \max_{\mathbf{z}} (\mathbf{z}^T \mathbf{a}), \quad \mathbf{z}^* \in \{0, 1\}^{n_1 n_2} \\ \text{s.t. } Z^* \mathbf{1} &\leq \mathbf{1} \quad \text{and} \quad (Z^*)^T \mathbf{1} \leq \mathbf{1}, \end{aligned} \quad (2)$$

where  $\mathbf{a} \in \mathbb{R}^{n_1 n_2}$  is a rowwise vectorized replica of  $A$  and  $Z^* \in \{0, 1\}^{n_1 \times n_2}$  is a row-wise reshaped replica of  $\mathbf{z}^*$ .

The constraints in (2) imply that a point  $\mathbf{x}_i \in S_1$  can only be matched to a single point in  $S_2$  or not matched at all. The same applies to each point  $\mathbf{y}_j \in S_2$ . Equation (2) can be optimally solved by the Hungarian algorithm [31] or approximated by Dynamic Programming [5].

In pairwise assignments, we are given a pairwise affinity measure  $\Omega_2$  that scores the simultaneous matching of  $c_i$  and  $c_j$ ,

$$\Omega_2 = \Omega_2(c_i, c_j),$$

implying that  $\mathbf{x}_i$  is matched to  $\mathbf{y}_{i'}$  and  $\mathbf{x}_j$  to  $\mathbf{y}_{j'}$  simultaneously. Pairwise affinities can encode geometric properties such as *local isometry*,

$$\begin{aligned} \Omega_2(c_i, c_j) &= \Omega_2(\{\mathbf{x}_i, \mathbf{y}_{i'}\}, \{\mathbf{x}_j, \mathbf{y}_{j'}\}) \\ &= \exp - \frac{1}{\varepsilon^2} (\|\mathbf{x}_i - \mathbf{x}_j\|_2 - \|\mathbf{y}_{i'} - \mathbf{y}_{j'}\|_2)^2, \end{aligned} \quad (3)$$

where  $\varepsilon > 0$  is the kernel bandwidth. The affinity matrix  $A$  is given by

$$A((i-1)n_2 + i', (j-1)n_2 + j') = \Omega_2(c_i, c_j),$$

and the optimal assignment is given by the one maximizing the sum of corresponding pairwise affinities

$$C^* = \max_C \arg \sum_C \Omega_2(c_i, c_j)$$

adhering to the same set of constraints as in (2).

This yields the following binary optimization problem:

$$\begin{aligned} \mathbf{z}^* &= \arg \max_{\mathbf{z}} (\mathbf{z}^T A \mathbf{z}), \quad \mathbf{z}^* \in \{0, 1\}^{n_1 n_2} \\ \text{s.t. } Z^* \mathbf{1} &\leq \mathbf{1} \quad \text{and} \quad (Z^*)^T \mathbf{1} \leq \mathbf{1}, \end{aligned} \quad (4)$$

where  $\mathbf{z}$  and  $Z$  are the same indicator vector/matrix pair as in (2), and  $A \in \mathbb{R}^{n_1 n_2 \times n_1 n_2}$ . The binary quadratic optimization problem in (4) is  $np$ -complete. Leordeanu and Herbert [22] showed how to apply spectral relaxation to the pairwise

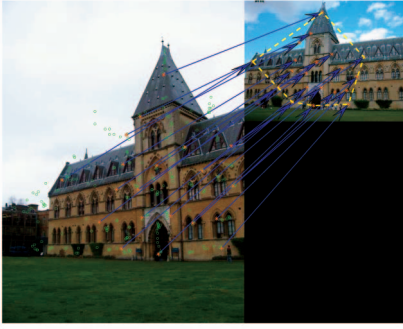


Fig. 1. Image registration by high order matching. The images were taken from the Oxford Buildings data set [32]. The right image was downscaled by a factor of two. Due to the scale differential the images cannot be matched by pairwise affinity measures.

HOA and derived an efficient and robust computational solution by way of spectral relaxation

$$\mathbf{w}^* = \arg \max_{\mathbf{w}} \frac{\mathbf{w}^T A \mathbf{w}}{\mathbf{w}^T \mathbf{w}}, \quad \mathbf{w} \in \mathbb{R}^{n_1 n_2}. \quad (5)$$

Equation (5) is solved by computing the leading eigenvalue and corresponding eigenvector of  $A$ . In point matching it is common to compute the affinity using a Gaussian kernel as in (3), which guarantees that  $A$  is symmetric and non-negative. Thus, by the Perron-Frobenius theorem, we have that the leading eigenvalue and eigenvector  $\mathbf{w}^*$  of  $A$  are known to exist and  $\mathbf{w}^*$  is nonnegative. Given the continuous solution  $\mathbf{w}^*$ , Leordeanu and Herbert [22] suggest discretizing  $\mathbf{w}^*$  by a greedy approach and deriving the indicator vector  $\mathbf{z}^*$ . The assignment constraints in (4) are ignored in the spectral relaxation step (5) and induced during the discretization step.

*Partial matching* implies that only subsets of size  $n \leq \min(n_1, n_2)$  of  $S_1$  and  $S_2$  can be matched. This is of particular interest in applications where the common set is embedded in clutter. In applications such as image registration, it is possible to restrict the space of potential assignments of each point  $\mathbf{x}_i \in S_1$  by using *local descriptors* [29]. These characterize each point and allow us to search for its  $K \ll n_2$  nearest neighbors in  $S_2$ . This reduces the dimensionality of the terms in (5) to  $A \in \mathbb{R}^{n_1 K \times n_1 K}$  and  $\mathbf{w}^* \in \mathbb{R}^{n_1 K}$ .

Although pairwise matching was found to be instrumental [6], [13], [16], some applications require high order affinities. For instance, consider the point sets depicted in Fig. 1. The local isometric matching in (3) will fail to register these images, as it is susceptible to the scale differences between the sets of points in each image. Using triplets affinities as in Fig. 2, we can match triangles and thus define a scale invariant similarity measure. This is the core motivation of our work.

In this work, we present and rigorously justify a computational approach to  $m$ -order high order matching. As  $m$ -order affinities are represented by  $m$ -order tensors, we denote our scheme Tensor-HOA. In particular, we present the following contributions:

**First**, we extend the probabilistic interpretation of hypergraph matching by Zass and Shashua [40] to derive a novel *spectral* high order matching scheme that is based on rank-one approximation (ROA) of tensors, by way of tensor

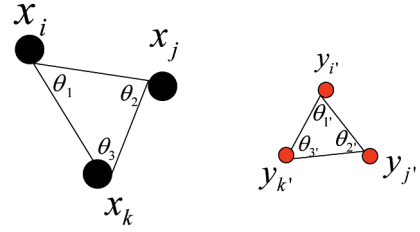


Fig. 2. Scale invariant matching using high order affinities. The two triangles are differentiated by an apparent scale change. Matching using pairwise affinities will fail, while high order matching based on triplets will measure the discrepancy in the angles and will thus be scale invariant.

eigendecomposition. We discuss the numerical attributes and downsides of such decompositions and propose a dual marginalization-decomposition scheme that reduces an  $m$ -order ROA problem to a second order ROA problem that can be solved efficiently and optimally by matrix eigendecomposition. This improves the matching accuracy and robustness and allows to reduce the memory storage required for the HOA as that is a fundamental obstacle to the feasibility and practical use of high order matching schemes.

**Second**, we utilize recent results in random matrix theory to sparsify the affinity tensor  $T_m$ . Thus, we are able to accurately compute the ROA of  $T_m$  while computing a small random subset of its elements. We show this scheme to be particularly appropriate for sparse tensors, such as the affinity tensor used by the HOA.

**Last**, we show that the discretization step of the relaxation is essentially the solution of a linear assignment problem and study different approaches for its computation.

This paper is organized as follows: Section 2 discusses previous results on graph matching and presents the Tensor-HOA scheme in Section 3. A probabilistic justification of the Tensor-HOA scheme is presented in Section 3.2, which paves the way for a dual marginalization-spectral matching scheme that improves on the Tensor-HOA. The Sparse Tensor-HOA is discussed in Section 3.3. Our approach is experimentally verified in Section 4 by applying it to synthetic as well as real data. Concluding remarks and future extensions are discussed in Section 5.

## 2 RELATED WORK

A myriad of algorithms were proposed for matching graphs and sets of point in  $\mathbb{R}^d$ , and a comprehensive survey was given by Conte et al. [9]. The first class of algorithm solves the bipartite graph matching problem or, equivalently, the LAP, as in (2). One of the first of such algorithms for point matching was proposed by Scott and Longuet-Higgins [35]. Their method solves the one-to-one matching by minimizing the sum of squared distances between matched points in both sets. It introduces a spectral formulation by computing a Gaussian-weighted affinity matrix  $A_{i,j} = \exp(-\|\mathbf{x}_i - \mathbf{y}_j\|^2/\epsilon^2)$ .  $A$  is replaced by  $P = UV$ , where  $U$  and  $V$  are matrices whose columns are the left and right singular vectors of  $A$ . The largest entries of  $P$  indicate strongly coupled points. This scheme implicitly assumes that  $A$  is an empirical approximation of the one-to-one assignment matrix  $\hat{A}$ , for which we have  $\hat{A}\mathbf{1} = \hat{A}^T\mathbf{1} = \mathbf{1}$ . It

was observed by Cour et al. [10] that this spectral decomposition acts as a projection operator into the space of assignment matrices.

The Graduated Assignment algorithm of Gold and Rangarajan [13] was one of the first to solve the quadratic assignment problem (QAP) by relaxing the constraint  $\mathbf{z}^* \in \{0, 1\}^{n_1 n_2}$  in (4) to  $\mathbf{w} \in \mathbb{R}^{n_1 n_2}$ . The derivative of the relaxed QAP is computed and an iterative update scheme is derived. The relaxation in this scheme boils down to a power iteration and thus precedes [22]. In addition, the authors introduce a stretching operator that iteratively increases high soft assignment values and decreases lower ones. The stretching is controlled by a continuation parameter, annealed after each iteration. In Section 3.2, we show this scheme to be an Estimate Maximize (EM) estimate of the soft assignments.

Maciel and Costeira [27] formulated pairwise matching as a constrained integer optimization problem with a concave optimization scheme, whose complexity is not polynomial and thus is computationally slow. Cour et al. [10] introduced two valuable extensions to Leordeanu's work. First, they introduced affine constraints into the spectral decomposition that encode the one-to-one matching constraints. In Leordeanu's work, these constraints were overlooked at the spectral decomposition step and imposed in the discretization step. Their second contribution is to apply bistochastic normalization to the Edge Similarity Matrix, which is an equivalent representation of the pairwise affinity matrix.

Torresani et al. [38] proposed a graph matching scheme they denote as *dual decomposition* for solving the QAP. They use the Nonlinear Inverse Optimization algorithm [25] to self-tune the parameters of the matching scheme. The approach was shown to be more robust than spectral relaxation, but slower by two orders of magnitude.

The work of Zass and Shashua [40] inspired our probabilistic analysis. They were the first to present a probabilistic framework for hypergraph matching, by assuming that different assignments are statistically independent. This builds upon their previous results on the connection between low-rank tensors and conditional independence [36]. The high order formulation represented by tensors is shown to encode high order geometric invariants such as scale and affine invariants. Zass and Shashua also present two contributions that constitute a high order graph matching algorithm: First, they marginalize the high order tensor into a one-dimensional probability vector, thus avoiding the need for high order rank-one-approximation. This probability vector is refined by projecting it into the space of assignment vectors by minimizing a Bergman measure.

In this work, we extend their results to derive a *spectral* approach to high order matching. By analyzing the down-sides of high order eigendecompositions, we suggest a dual marginalization-spectral approach that outperforms the pure spectral scheme.

The work of Duchenne et al. [11] is of particular interest as they *independently* presented a spectral high order scheme similar to ours. They extend Leordeanu and Hebert's approach [22] by replacing the affinity matrix with an affinity tensor and using the High Order Power Iteration. They describe the construction of affinity tensors that can be

made scale, affinity, and projective-invariant. To deal with the increased computational complexity and storage, they propose to only consider triangles (for third-order affinities) that consist of close points in the source image ( $S_1$ ) and compute all of the triangles in the target image ( $S_2$ ).

High order matching was applied by Mammalian et al. [30] to matching corresponding moles in patient's skin at different scanning times. In order to measure the distances between moles in geodesic coordinates on the body surface, the image of the back is segmented and fitted to a surface model. The matching is then formulated by high order graph matching, where the affinity tensor consists of a combination of geometric and anatomical terms. This work exemplifies the applicability and flexibility of graph matching.

Hypergraphs were shown to be instrumental in high order clustering and classification, where the relationships between the objects of interest are more complex than pairwise. Zhou et al. [41] proposed using hypergraphs to represent such complex relationships and derived a spectral clustering approach for hypergraphs and transductive classification. They present the equivalent of a Normalized Cut on hypergraphs and a random walk interpretation, similar to previous results in pairwise clustering [37].

Govindu [15] and Agarwal et al. [3] proposed to explicitly represent high order geometric affinities by an affinity tensor. The affinities are the fitting error of a parametric geometrical models such as a conic or an affine motion. In [15], the affinity tensor is decomposed by first flattening it, as in the High Order SVD, and utilizing its supersymmetry to randomly subsample the flattened tensor and compute its eigenvectors using a subset of matrix. In [3], the hypergraph is reduced to a graph by Clique Averaging and is partitioned by spectral clustering.

Theoretical analysis of the graph Laplacians of hypergraphs was conducted by Agarwal et al. [2]. They analyze the structure of hypergraphs for unsupervised and semi-supervised learning and show how to reduce the hypergraphs to pairwise graphs represented by affinity matrices and their corresponding graph Laplacians.

Note that these works [2], [3], [15], [41] deal with classification and clustering, while our work solves the graph matching problem.

### 3 HIGH ORDER ASSIGNMENT

High order assignment is an extension of the pairwise formulation [22]. Given two sets of points in  $\mathbb{R}^d$  such that  $S_1 = \{\mathbf{x}_i\}_{i=1}^{n_1}$  and  $S_2 = \{\mathbf{y}_i\}_{i=1}^{n_2}$ , the  $m$ -order affinity measure  $\Omega_m$  quantifies the matching of  $m$  pairs of points

$$\begin{aligned}\Omega_m &= \Omega_m(c_{i_1}, \dots, c_{i_m}) = \Omega_m(i_1, \dots, i_m) \\ &= \Omega_m(\{\mathbf{x}_{i_1}, \mathbf{y}_{i'_1}\}, \dots, \{\mathbf{x}_{i_m}, \mathbf{y}_{i'_m}\}).\end{aligned}$$

For instance, with triplets matching we get

$$\Omega_m = \Omega_m(c_i, c_j, c_k) = \Omega_m(\{\mathbf{x}_i, \mathbf{y}_{i'}\}, \{\mathbf{x}_j, \mathbf{y}_{j'}\}, \{\mathbf{x}_k, \mathbf{y}_{k'}\}).$$

This is depicted in Fig. 2, and the affinity measure reflects the sort of matching we are aiming for. Local isometric matching, similar to the one used in [22], can be achieved by

$$\Omega_m(c_i, c_j, c_k) = \exp - \frac{\|\overline{\mathbf{x}_i \mathbf{x}_j} - \overline{\mathbf{y}_{i'} \mathbf{y}_{j'}}\| + \|\overline{\mathbf{x}_i \mathbf{x}_k} - \overline{\mathbf{y}_{i'} \mathbf{y}_{k'}}\| + \|\overline{\mathbf{x}_k \mathbf{x}_j} - \overline{\mathbf{y}_{k'} \mathbf{y}_{j'}}\|}{\varepsilon^2}, \quad (6)$$

where  $\overline{\mathbf{x}_i \mathbf{x}_j}$  is the length of the corresponding line segment. It was first shown by Zass and Shashua [40] that high order affinities can encode geometrical invariance, such as scale and affinity invariance (see Section 4.2). For instance, local scale invariance can be derived by computing the affinities  $\Omega_3$  of the triplets depicted in Fig. 2. Those are based on the difference in corresponding angles,

$$\Omega_3(c_i, c_j, c_k) = \exp - \frac{1}{\varepsilon^2} (\|\theta_1 - \theta_{1'}\| + \|\theta_2 - \theta_{2'}\| + \|\theta_3 - \theta_{3'}\|), \quad (7)$$

and are thus scale invariant.

The  $m$ -order affinities  $\Omega_m$  can be represented by an  $m$ -order tensor  $T_m$  such that

$$T_m(i_1, \dots, i_m) = \Omega_m(c_1, \dots, c_m).$$

For instance, in triplets assignments,  $T_3$  is given by a three-dimensional tensor,

$$T_3(i, j, k) = \Omega_3(c_i, c_j, c_k). \quad (8)$$

The assignments are then recovered by computing the assignment vector  $\mathbf{z}^* \in \{0, 1\}^{n_1 K}$  that maximizes the overall assignment affinity,

$$\mathbf{z}^* = \arg \max_{\mathbf{z}} \sum_{i_1, \dots, i_n} T_m(i_1, \dots, i_n) \mathbf{z}_{i_1} \mathbf{z}_{i_2} \dots \mathbf{z}_{i_n}, \quad \mathbf{z}^* \in \{0, 1\}^{n_1 K}. \quad (9)$$

In the triplets case, we get

$$\mathbf{z}^* = \arg \max_{\mathbf{z}} \sum_{i_1, \dots, i_n} T_3(i, j, k) \mathbf{z}_i \mathbf{z}_j \mathbf{z}_k, \quad \mathbf{z}^* \in \{0, 1\}^{n_1 K}. \quad (10)$$

The tensor  $T_m$  is nonnegative and symmetric, such that

$$T_m(\mathbf{i}) = T_m(i_1, \dots, i_m) = T_m(\mathbf{i}') \geq 0,$$

where  $\mathbf{i}'$  is any permutation of  $\mathbf{i}$ . For an  $m$ -order tensor, we get  $m!$  such permutations. For instance, for a three-way symmetric tensor,  $\mathbf{i} = (x, y, z)$  and

$$\begin{aligned} T_3(x, y, z) &= T_3(x, z, y) = T_3(y, x, z) \\ &= T_3(z, x, y) = T_3(z, y, x) = T_3(y, z, x). \end{aligned}$$

This implies that, instead of computing the  $(n_1 K)^m$  elements of  $T$ , it suffices to compute  $\frac{(n_1 K)^m}{m!}$  elements.

Solving (9) and (10) is known to be  $np$ -complete and, analogue to the pairwise case [22],  $\mathbf{z}^*$  can be estimated by computing the rank-one approximation (ROA) of  $T_m$ ,

$$T_m \approx \mathbf{w} \otimes_T \mathbf{w} \dots \mathbf{w} \otimes_T \mathbf{w} \triangleq \prod_{i=1..m} \otimes_T \mathbf{w}, \mathbf{w} \in \mathbb{R}^d, \quad (11)$$

where  $\otimes_T$  is the *tensor* product. This will be rigorously justified in Section 3.2. The assignment  $\mathbf{z}^*$  is derived by discretizing  $\mathbf{w}$  the same way it was done in the pairwise case [22]. We discuss some alternatives in Section 3.4.

The effectiveness of this scheme is experimentally verified in Section 4. But still, a few issues have to be discussed. First, in the pairwise case, the ROA is justified as the spectral relaxation of a  $np$ -complete problem [22]. Spectral relaxations of quadratic binary optimization problems are widely used and well understood, originating with the seminal work of Shi and Malik [37]. Unfortunately, this does not extend well to higher dimensions (tensors). The notions of ROA and eigendecomposition are different for tensors, from a theoretical as well as a numerical point of view.

To resolve these issues in the context of this work, we extend recent results by Zass and Shashua [40] on the probabilistic interpretation of affinity tensors. We show in Section 3.2 that the spectral decomposition is a proxy for the ROA of the affinity tensor  $T_m$ . The numerical aspects of tensor ROA are discussed in Section 3.1.

The second downside of the proposed HOA scheme is that practical assignment problems require extremely high memory storage and computational resources. For instance, in the image registration examples presented in Section 4, we match images using  $n = 500$  points, each having  $K = 4$  potential assignments. This results in an affinity tensor of dimensions  $(n_1 K)^m = 2000^3 = 8 \times 10^9$  elements. Utilizing the supersymmetry, it can be reduced to  $\frac{(n_1 K)^m}{m!} = 1.3 \times 10^9$  elements. Computing and storing such volumes of data might render this scheme useless. Fortunately, the affinity tensor  $T_m$  is sparse, as significant nonzero elements would be those for which all assignments are true. Hence, only  $\frac{1}{K^3} = 0.8\%$  of the affinity elements are expected to be nonzero. In practice, only 0.03 percent of the elements are nonzero. The increased sparsity is due to partial matching, as not all of the points  $\mathbf{x}_i \in S_1$  can be matched to points in  $S_2$  as some of them are due to clutter. The affinities of those clutter points will all be zero. To sparsify the affinity matrix numerically, we threshold it by  $O(10^{-5})$  as the affinities of true matches are typically of  $O(10^{-1})$ . Yet, without having to deal with clutter we could have used significantly fewer points. It follows that the more points one needs to match due to clutter, the sparser the affinity tensor is.

The common approach for further sparsifying the affinity tensor in image matching problems was proposed by Zass and Shashua [40] and Torresani et al. [38]. They propose computing the high order affinities only for pixels of close proximity within the image. Thus, only a small subset of the affinities have to be computed. This heuristic is inapplicable to general HOA problems not involving images. We present an alternative general random sparsification approach in Section 3.3.

In the following sections, we discuss the tensor ROA and present several extensions to the basic scheme described above. These extensions make it computationally feasible in terms of storage and computational complexity, allowing us to run the image matching setup described above in less than two seconds.

### 3.1 Rank One Approximation of Nonnegative Symmetric Tensors

The study of tensors from an algorithmic as well as applicative points of view has recently gained significant attention [19], [33]. By construction, the affinity tensor is nonnegative and symmetric, and we aim to compute its ROA. In the pairwise

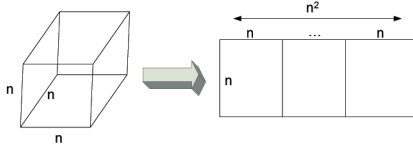


Fig. 3. Tensor unfolding.

assignment case, we were able to apply the Perron-Frobenius theorem to the affinity matrix  $T_2$ . It guarantees the existence of a leading eigenvector and that all of its elements would be nonnegative. Using the Eckart-Young Theorem, it follows the leading eigenvector would also provide the optimal ROA. Numerically, the leading eigenvector can be computed by the Power Method, which is robust and globally convergent.

Unfortunately, these properties do not carry over to tensors. A Perron-Frobenius-like theorem for tensors was discussed by Lim [24] and the uniqueness of the leading eigenvector was proven by Chang et al. [7]. But, the leading eigenvector is not the optimal ROA [18]. Yet it provides a good approximation of it.

From a numerical perspective, there is a lack of robust ROA schemes, such as the matrix eigendecomposition schemes. A high order SVD algorithm was proposed by Lathauwer et al. [20] for asymmetric tensors, while a tensor ROA scheme based on the Power method (HOPM) was suggested by the same authors in [21]. However, the HOPM is not convergent for symmetric tensors, as claimed in [21] and demonstrated in [17]. A thorough survey of tensor decompositions was provided by Kolda and Bader [19].

We used a straightforward ROA scheme based on the HOPM [21]. We initialize the computation by unfolding the tensor into a matrix, as exemplified in Fig. 3 for an order-3 tensor. In that case, the leading left singular vector of the unfolded tensor  $T_u \in \mathbb{R}^{(n_1 K) \times (n_1 K)^2}$  coincides with  $\mathbf{x}$ , which is the ROA of  $T_m$ . The right singular vector is given by  $[\mathbf{x}^T \dots \mathbf{x}^T]^T \in \mathbb{R}^{(n_1 K)^2}$ . In general, given a rank-one tensor  $T_m$ , the unfolding results in a matrix  $T_u \in \mathbb{R}^{(n_1 K) \times (n_1 K)^{m-1}}$  with a left singular vector  $\mathbf{x}$ . As the affinity tensor  $T_m$  is symmetric, any axis can be chosen as the folding axis.

Due to the asymmetric dimensions of the matrix  $T_u$ , it is better to compute the leading eigenvector of  $T_u T_u^T \in \mathbb{R}^{(n_1 K) \times (n_1 K)}$  that identifies with  $\mathbf{x}$ . Denote this initial estimate  $\mathbf{x}_0$ . Given  $\mathbf{x}_0$ , we apply two to three more HOPM iterations. This numerical scheme insures that the solution is nonnegative, as  $\mathbf{x}_0$  will be nonnegative due to the Perron-Frobenius theorem applied to the matrix  $T_u T_u^T$ , and the HOPM consists of multiplications by the nonnegative elements of  $T_m$ .

### 3.2 Probabilistic Interpretation and Marginalized Tensor-HOA

In this section, we extend the probabilistic analysis of hypergraph matching by Zass and Shashua [40] to spectral matching. Zass and Shashua proposed a probabilistic model for pairwise matching, where the symmetric affinity tensor  $T_m$  is modeled by the *joint probability* of the assignments

$$T(\mathbf{i}) = P(\mathbf{i}), \quad \mathbf{i} = [i_1, i_2 \dots i_n].$$

Examining (6) and (7), it follows that  $0 \leq P(\mathbf{i}) \leq 1 \forall \mathbf{i}$  and that  $P(\mathbf{i}) \approx 1$  implies that all of the point correspondences are true. They further assume that the different assignments are statistically independent and show that the affinity tensor can be decomposed as

$$T_m = \prod_{i=1..m} \otimes_K \mathbf{P}, \quad \mathbf{P} \in [0, 1]^{n_i}, \quad (12)$$

where  $\otimes_K$  is the Kronecker product.

Equation (12) constructs a matrix that can not be used for spectral matching. In particular, in the HOA problem, applying (12) results in an affinity matrix rather than an affinity tensor  $T_m$ , as in (11).

Hence, we propose to apply tensor product to construct the tensor  $T_m$ ,

$$T_m = \prod_{i=1..m} \otimes_T \mathbf{P}, \quad \mathbf{P} \in [0, 1]^{n_i}, \quad (13)$$

where  $\otimes_T$  is a tensor product. It follows that the true assignment probability is given by the ROA of  $T_m$ , without having to relate it to spectral relaxations, or discrete optimization. This justifies the HOA scheme based on the eigendecomposition of  $T_m$ , which is equivalent to the one proposed by Duchenne et al. [11].

Following Section 3.1, we suggest avoiding computing the ROA of the tensor  $T_m$  due to its numerical inaccuracy. Instead, we utilize the marginalization proposed by Zass and Shashua [40]. But instead of marginalizing  $T_m$  down to a vector, as in their work, we propose using *partial marginalization* by marginalizing  $T_m$  down to  $T_2$  (a matrix) and computing its ROA by eigendecomposition. The eigendecomposition of matrices is optimal (Eckart-Young Theorem) and numerically stable [14].

Recall that the affinity tensor is an approximation of the joint probability [40]:

$$\begin{aligned} T_{m-1} &= \sum_{i_1} T_m(i_1, i_2 \dots i_m) \\ &= \sum_{i_1} P(i_1, i_2 \dots i_m) = P(i_2 \dots i_m). \end{aligned}$$

$T_{m-1}$  is a symmetric tensor of order  $m-1$  whose ROA identifies with the ROA of  $T_m$ . The marginalization is true for *any* joint probability function and does not assume statistical independence among the different assignments.

### 3.3 Randomly Sparsified High Order Spectral Matching

The affinity tensor is a sparse low rank tensor and so is the unfolded matrix  $T_u \in \mathbb{R}^{n \times n^{m-1}}$  discussed in Section 3.1, which is of rank one in the noise-free case. Hence, computing the leading left singular vector  $\mathbf{x}$  is an over-determined problem. For instance, Govindu [15] proposed to subsample (erase) some of the columns of  $T_u$  while retaining  $\mathbf{x}$  as the leading left singular vector. In image matching [11], [40], the particular structure of the problem can be utilized to prune the high order affinities a priori by only computing the affinities of close points.

In this section, we propose a general approach to randomly sparsifying  $T_u$  and equivalently the original tensor  $T_m$ . This provides better accuracy than subsampling the columns of  $T_u$  [15] and can be applied to any high order matching problem.

In particular, in image matching applications, it can be used alongside the spatial sparsification as in [11], [40].

There is a plethora of results on fast approximation algorithms for large low-rank matrices in general and singular value decompositions in particular [23], [34]. The work of Achlioptas and McSherry [1] is of particular interest as it provides the mathematical foundations for approximating the spectrum if a matrix given its sparsified replica. The core idea is that sparsifying a large low dimensional matrix is equivalent to adding a random matrix  $E$  whose entries are independent random variables with zero-mean and bounded variance:

$$\hat{T}_u = T_u + E.$$

The eigenvalues of such random matrices  $E$  are known to be of bounded magnitude [8] and do not influence the computation of the leading eigenvalues and eigenvectors of  $\hat{T}_u$ . The more elements of  $T_u$  are erased, the larger the eigenvalues of the matrix  $E$ . Consider the eigendecomposition  $E = \sum_i \lambda_i \phi_i \phi_i^T$ . The more nonzero elements in  $E$ , the larger its  $L_2$  norm and the larger its eigenvalues  $\lambda_i$  will be (recall that  $\|\phi_i\| = 1$ ). Hence, this approximation is appropriate for sparse matrices  $T_u$ , whose further sparsification is equivalent to adding a noise matrix  $E$  with relatively small eigenvalues.

In the context of this work,  $T_u$  is sparsified by a factor  $Q$  during its construction by drawing a random number  $t \sim U[0, 1]$  at each affinity entry and computing the affinity value only if  $t < \frac{1}{Q}$ . In order to retain the symmetry of  $T_u$ , we apply the sparsification appropriately by making the sparsity pattern symmetric.

### 3.4 Soft Assignment Refinement and Discretization

So far we have suggested a high order matching scheme that results in a vector of soft assignments  $\mathbf{w}^* \in \mathbb{R}^{n_1 K}$ . Before discretizing  $\mathbf{w}^*$  to yield the hard assignment  $\mathbf{z}^*$ ,  $\mathbf{w}^*$  can be refined by projecting it onto the space of soft assignment vectors. Cour et al. [10] utilize the spectral matching algorithm of Scott and Longuet-Higgins [35] as a spectral approach to inducing the matching constraints. First,  $\mathbf{w}^*$  is reshaped as  $W^* \in \mathbb{R}^{n_1 \times K}$  and the projection  $\hat{W}^*$  is given by

$$\hat{W}^* = \arg \min_W \|W^* - W\|_2, \text{ s.t. } W\mathbf{1} = \mathbf{1} \text{ and } W^T \mathbf{1} = \mathbf{1}. \quad (14)$$

Zass and Shashua [40] solve a similar problem as in (14), but the similarity of the assignment matrices is measured by the relative entropy measure.

Following Section 3.2, the soft assignment vector  $\mathbf{w}^*$  (with or without refinement) identifies with the assignment probability  $P$ . We aim to compute the hard assignment  $\mathbf{z}^* \in \{0, 1\}^{n_1 K}$  that maximizes the overall assignment probability

$$\begin{aligned} \mathbf{z}^* &= \arg \max_{\mathbf{z}} (\mathbf{z}^T \mathbf{w}^*) = \arg \max_{\mathbf{z}} (\mathbf{z}^T P) \\ &= \arg \max_{\mathbf{z}} \sum_{z_k=1} P(k), \mathbf{z}^* \in \{0, 1\}^{n_1 K} \\ &\text{s.t. } Z^* \mathbf{1} \leq \mathbf{1} \quad \text{and} \quad (Z^*)^T \mathbf{1} \leq \mathbf{1}, \end{aligned} \quad (15)$$

where  $Z^* \in \{0, 1\}^{n_1 \times K}$  is a rowwise reshaped replica of  $\mathbf{z}^*$ .

The greedy algorithm used by Leordeanu and Herbert [22] provides an approximate solution of (15) by iteratively picking the highest element in  $\mathbf{w}^*$  and inducing the

assignment constraints. This can also be optimally solved by the Hungarian algorithm [31].

## 4 EXPERIMENTAL RESULTS

We applied the proposed approach to synthetically generated random graphs as well as real images and sequences. In the synthetic graphs simulations, we followed the experimental framework used by Zass and Shashua [40]. It allows us to quantify the accuracy and resiliency of the proposed schemes and compare it to contemporary state-of-the-art algorithms by applying them to millions of randomly generated graphs. The same synthetic graph, having a known ground truth, is used as input to all of the different matching schemes at a time. We also experiment with the registration of real images to show the applicability of the Tensor-HOA to image matching. Last, we analyze the matching of the *Hotel* and *House* sequences. We concentrate on using triplets affinities manifested by third-order tensors, as those are the most practical.

### 4.1 Matching of Random Synthetic Graphs

In this set of trials, we measure the accuracy and resiliency of our approach to different spatial deformations: noise, scale, and outliers, both at the source and the target sets. In each trial, we generated a set of 20 random points  $S_1 = \{\mathbf{x}_i\}_{i=1}^{20}$ ,  $\mathbf{x}_i \in \mathbb{R}^2$ , and  $\mathbf{x}_i \sim U[0, 1]^{2 \times 1}$ . We denote this randomly generated set as the *source set*.

In each trial, a particular deformation (noise, scale, or outliers insertion) is applied to  $S_1$ . We denote the distorted source set as the *target set*  $S_2 = \{\mathbf{y}_i\}_{i=1}^{20}$ , and apply different state-of-the-art matching schemes (including our own) to match  $S_1$  to  $S_2$ . By construction, we have that  $\mathbf{x}_i$  corresponds to  $\mathbf{y}_i$  and this acts as the ground truth. We measure the matching accuracy as the number of correctly matched points divided by the total number of points that could potentially be matched. Note that in the outliers test, not every point  $\mathbf{x}_i \in S_1$  has a corresponding point in  $S_2$ . In all simulations, we used the triplets affinity measure given in (7) with the same kernel bandwidth  $\varepsilon = \frac{\pi}{15}$ . The affinity tensor was 10 percent full on average while thresholding the affinity tensor by  $10^{-5}$ .

We tested various algorithmic setups that are detailed in Table 1, where each setup is made up of a different combination of the computational components. For a given graph distortion (i.e., scale, noise variance, number of outliers), we repeat the same experiment 100 times by generating 100 random sets  $S_1$  (source graphs) and applying the distortion. We report the mean accuracy over the different trials.

First, we tested the robustness of our algorithm to additive random noise by computing the *target set*  $S_2$  as

$$\mathbf{y}_i = \mathbf{x}_i + \mathbf{n}_i, \quad \forall \mathbf{x}_i \in S_1, \quad \mathbf{n}_i \sim N(0, \sigma).$$

In applications such as image matching, this simulates image distortions, as well as the localization inconsistencies of interest points detector. In this trial the matching is one-to-one. Fig. 4 depicts the accuracy of the various schemes with respect to  $\sigma$ . In real matching scenarios, descriptors can be used to prune the set of possible assignment per point  $\mathbf{x}_i \in S_1$ . Hence, we applied the different schemes with  $K = 5$  and  $K = 10$ . Using  $K = 5$  corresponds to having highly



TABLE 1  
The Different Matching Schemes

Notation	Affinity	Margin.	Rank one approximation	$T_1$ Refinement
FA+TE	$T_3$ full affinity	none	Tensor RON + GradAssign	ProbOpt
FA+M2	$T_3$ full affinity	$T_2$ (matrix)	GradAssign	ProbOpt
FA+M1	$T_3$ full affinity	$T_1$ (vector)	none	ProbOpt
SA2+TE	$T_3$ sparse affinity 50%	none	Tensor ROA+GradAssign	ProbOpt
SA2+M2	$T_3$ sparse affinity 50%	$T_2$ (matrix)	GradAssign	ProbOpt
SA2+M1	$T_3$ sparse affinity 50%	$T_1$ (vector)	none	ProbOpt
SA5+TE	$T_3$ sparse affinity 20%	none	Tensor ROA+GradAssign	ProbOpt
SA5+M2	$T_3$ sparse affinity 20%	$T_2$ (matrix)	GradAssign	ProbOpt
SA5+M1	$T_3$ sparse affinity 20%	$T_1$ (vector)	none	ProbOpt
ProbOpt [40]	$T_3$ full affinity	$T_1$ (vector)	none	ProbOpt
Spectral [22]	$T_2$ full affinity	none	EIGS	none
GradAssign [13]	$T_2$ full affinity	none	GradAssign	none

*Greedy discretization was used as the last step in all schemes.*

discriminative local features, able to significantly limit the number of potential assignments per point in  $S_1$ . The results depicted in Figs. 4a and 4b show that all of the schemes performed well, except for those using an aggressively sparsified affinity matrix (SA5+TE, SA5+M2, SA5+M1). In contrast, in image registration (Section 4.2), we sparsified the affinity tensor by a factor of 10 and were able to successfully register the images. This is due to a significant difference in the sparsity of the affinity tensors in both applications and is further discussed in the next section.

The superior numerical stability of the matrix eigendecomposition compared to the tensor ROA is evident. Thus, the FA+M2 scheme outperforms the FA+TE, and SA2+M2 outperforms the SA2+TE scheme.

We compare the matching performance of the proposed approach to state-of-the-art schemes in Fig. 5. This is the same setup as in Fig. 4, but for the sake of clarity, we only show some of the Tensor-HOA formulations. The results of matching using  $K = 10$  potential matches per  $\mathbf{x}_i \in S_1$  are reported in Fig. 5a. It follows that the Tensor-HOA schemes outperform all of the pairwise schemes where the Graduated Assignment was the best. Fig. 5b repeats this trial with  $K = 20$ . This implies that there is no pruning of potential matches and that the assignment problem is made more difficult. In this setup the Tensor-HOA outperforms the Graduated Assignment and ProbOpt by 50 percent, while the pairwise spectral approach fails completely.

Scale invariant matching was our core motivation for developing the Tensor-HOA, as state-of-the-art pairwise matching schemes [13], [22] are unable to match sets of

points related by scale changes. We drew 100 sets of points  $S_1$  and induced a scale change  $\Delta S$  and added noise

$$\mathbf{y}_i = \Delta S \cdot \mathbf{x}_i + n_i, \quad \forall \mathbf{x}_i \in S_1, \quad n_i \sim N(0, 0.05).$$

The triplets affinity measure in (7) is scale invariant and can thus be applied. The results are shown in Fig. 6, where it follows that the tensor-based schemes overcame the scale change. As in the noise resiliency trials, for  $K = 5$  (Fig. 6a), all schemes performed similarly down to a few percents of accuracy. For  $K = 10$  (Fig. 6b), we witness the same phenomenon as in the noise trials, where the aggressive sparsification (SA5) reduces the accuracy. The accuracy of the pairwise schemes reported in Fig. 7 quickly drops to that of random matching, where using  $K = 10$  as (Fig. 7a) implies that random assignments will have an accuracy of 10 percent. The same applies to Fig. 7b.

Partial matching is of particular interest, as one-to-one matching is rarely present in real matching scenarios.

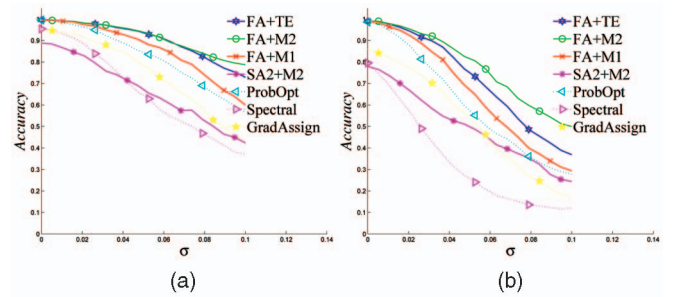


Fig. 5. Graph matching simulations with additive noise. We added WGN to a set of 20 uniformly randomly spread points. The points were registered with (a)  $K = 10$  and (b)  $K = 20$  potential matches per point.

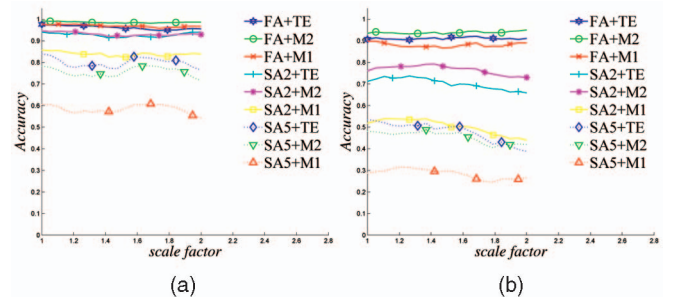


Fig. 6. Graph matching simulations with varying scale and noise. A set of 20 uniformly randomly spread points was rescaled. The points were registered with (a)  $K = 5$  and (b)  $K = 10$  potential matches per point.

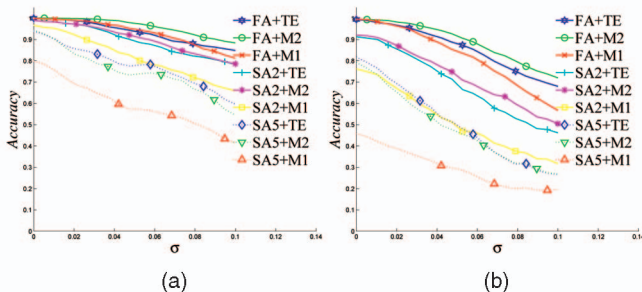


Fig. 4. Graph matching simulations with varying additive noise. We added WGN to a set of 20 uniformly randomly spread points. The points were registered with (a)  $K = 5$  and (b)  $K = 10$  potential matches per point.

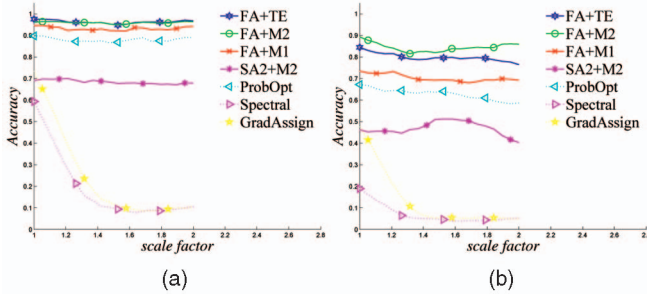


Fig. 7. Graph matching simulations with varying scale and noise. A set of 20 uniformly randomly spread points was rescaled. The points were registered with (a)  $K = 10$  and (b)  $K = 20$  potential matches per point.

Consider, for instance, the images used in Section 4.2. A feature points detector will detect points in one image, many of them lacking corresponding points in the other one. As before, we define an experimental set up that simulates the addition of outliers to both source and target sets.

We generate random sets with 20 points and add 10 random outliers to the source set  $S_1$ . Those have no correspondences in the second graph. Their potential  $K$  matches per point are picked randomly. For the inliers, we insert the true match as one of the  $K$  potential matches. We also added a varying number of outliers to the target set and random noise  $N(0, 0.05)$ .

The results are reported in Figs. 8 and 9. As before, the Tensor HOA schemes performed well for  $K = 5$ . The results shown in Fig. 8a do not vary much among the different schemes. For  $K = 10$ , the sparsification hampers the accuracy again.

## 4.2 Image Matching

The registration of images related by significant spatial deformation in general and scalings in particular is an unresolved challenge in computer vision. This task requires overcoming scaling, noisy feature points localization, and outliers present in the source as well as the target image. All image pairs used in this section are real images. In order to increase the scale differential, we downsampled some of them.

In order to implement an image registration scheme by way of point assignment, we first have to represent the image as a set of interest points. Thus, we turn to image modeling by means of *local features* [26], [28]. These can be used to represent the image by a sparse set of salient points  $\{x_i\}$  detected by a *detector*. Each interest point is represented by a vector of parameters denoted a *descriptor*. The descriptors are

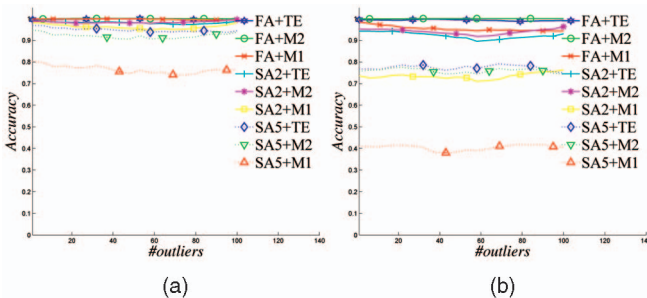


Fig. 8. Graph matching simulations with added outliers. The points were registered with (a)  $K = 5$  and (b)  $K = 10$  potential matches per point.

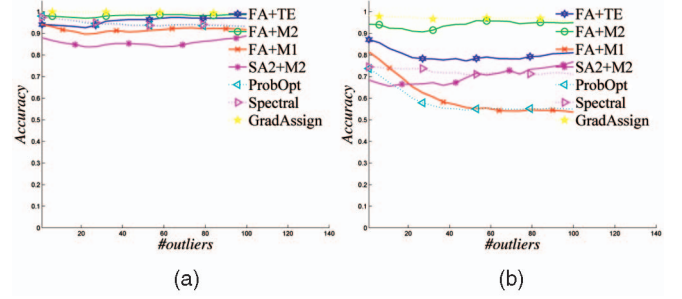


Fig. 9. Graph matching simulations with added outliers. The points were registered with (a)  $K = 10$  and (b)  $K = 20$  potential matches per point.

scale and rotation invariant. This is achieved by computing a *dominant scale* and *dominant angle* of each interest point  $x_i$  [26], [28]. Those allow normalization of the computation of the descriptors with respect to rotation and scale.

We detected 500 interest points in each image and computed their SIFT descriptors [26]. In each figure, we mark a subset of those on the images. One of the input images was chosen to contain the points  $S_1 = \{x_i\}_{i=1}^{500}$  while  $S_2 = \{y_i\}_{i=1}^{500}$  were taken in the other. In all registrations, we used a constant number of  $K = 4$  potential correspondences for each point  $x_i$ , chosen as the  $K$  points in  $S_2$  with the most similar SIFT descriptors.

As image registration requires scale invariant matching, we used the scale invariant triplets affinity measure given in (7) with the same kernel bandwidth  $\varepsilon = \frac{\pi}{15}$ . Such an affinity measure cannot be implemented with any pairwise scheme [13], [22] and is thus unique to HOA schemes.

The affinity tensor was thresholded by  $10^{-5}$ . This yielded an affinity tensor that was, on average,  $5 \times 10^{-4}$  full. To further sparsify it by a factor of 10, we applied the random sparsification scheme (Section 3.3), and got a tensor that was only  $5 \times 10^{-5}$  full. In contrast, in the points matching trials in Section 4.1, the affinity tensor was  $10^{-1}$  full on average. Hence, the sparsification was equivalent to adding a noise matrix  $E$  with  $O(10^{-1} \cdot (n_1 K)^2)$  nonzero elements, compared to  $O(10^{-4} \cdot (n_1 K)^2)$  such elements in this section. Following Section 3.3, this matrix  $E$  would have larger eigenvalues, and thus corrupt the ROA approximation.

The first example of image registration is given in Fig. 10, where the scale factor is approximately 2. It is typical for images with such scale changes to have a relatively small common support, which translates to a large number of interest points that are outliers.

The registration of a pair of images related by a scaling factor of 2.8 and a change in the view angle is depicted in



Fig. 10. Fully automatic registration of images with a scaling factor of 2. Due to the significant scaling, the common image parts are small, resulting in many interest points being outliers. The green circles are a subset of the local feature used.





Fig. 11. Registration of images with a scale change of 2.8. Due to the different view angle and the projective transformation, the scaling changes along the images. The green circles are a subset of the local feature used.



Fig. 12. Registration of image with significant scale changes. We are able to recover a scale change of 6 in (a), but fail to estimate a scale of 8 in (b). Both use the same image as in Fig. 11. The green circles are a subset of the local feature used.



Fig. 13. Registration of images related by a scale factor of 2 and a significant projective distortion due to the difference in the viewing angle. The green circles are a subset of the local feature used.

Fig. 11. The successful registration was able to overcome the significant variation in the viewing angle that induced a projective transformation.

We further studied the scale invariance by increasing the scale differential of the image pair in Fig. 11. These results are shown in Fig. 12. We were able to successfully register the image in Fig. 12a having a scale factor of 6, but failed to estimate a scale factor of 8 in Fig. 12b. Since the common support and transformations between the image pairs in Figs. 12a and 12b are the same as those in Fig. 11, we attribute the failure to a break-down of the scale-invariance of the local descriptors.

The registration of images related by significant affine deformations was studied in Figs. 13 and 14. In Fig. 13, we successfully aligned images of planar objects under different viewing angles and a scale factor of 2.

In Fig. 14, we match Graffiti images taken from the Oxford VGG database.<sup>1</sup> This is a set of six images where the affine distortion is increasing with respect to the first image of the series. We added an additional scaling of 2. The successful

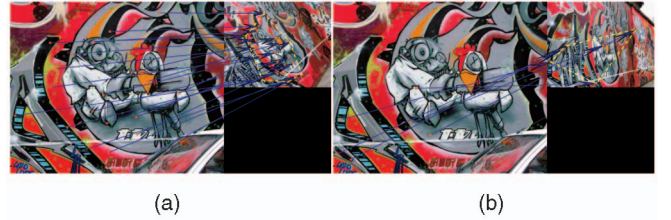


Fig. 14. Matching images from the Graffiti series. We downsampled the target image by a factor of two. In (a), we successfully matched the first image to the fourth one. In (b), we failed to match the first image to the fifth one, which has a more significant distortion. We used regular SIFT descriptors to match the images. The green circles are a subset of the local feature used.

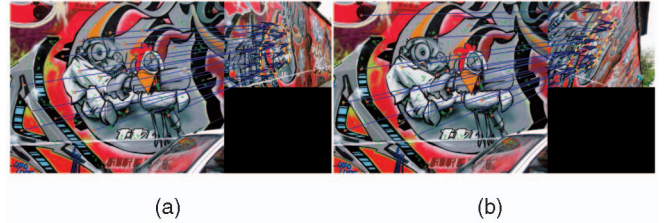


Fig. 15. Image registration using the Tensor-HOA and affine invariant image features. In (a), we successfully registered the first image in the Graffiti series to the fifth and, in (b), we registered the first to the sixth. The green circles are a subset of the local feature used.

registration of the first and third images in the series is depicted in Fig. 14a, while Fig. 14b shows the failure to register the first and fourth images. As in the registration failure in Fig. 12b, we attribute that to a reduction in the accuracy of the local descriptors due to the deformation. To further elucidate that, we applied affine invariant SIFT features along side our Tensor HOA in Fig. 15. We successfully matched the first image in the Graffiti series to the fifth and sixth images, where, as before, we downsampled the target image by a factor of 2. The relative deformation of those images is so severe that it was difficult to verify their accuracy visually.

To conclude, the proposed scheme was successfully applied to a variety of difficult image registration tasks. It seems that, in practice, its accuracy is only limited by the resiliency and accuracy of the local features. Due to the large number of outliers present in such images, the affinity tensor is sparse up to  $O(10^{-4})$  nonzero elements and can be further sparsified by applying random sampling.

### 4.3 Sequence Matching

We applied our approach to the CMU *Hotel* and *House* sequences.<sup>2</sup> These were used in multiple works [11], [38] and provide a baseline for comparison. In order to evaluate the matching accuracy, we tracked landmark feature points that were manually labeled and tracked in *all* frames. This allows comparing the performance of the different schemes over a varying temporal baseline—the larger the temporal baseline (differential) between the frames, the larger the relative deformation and the more difficult the matching. We matched each frame to the frames succeeding it and computed the average matching error per temporal baseline.

As in the noise tests in the previous section, we utilized the number of possible assignments  $K$  as a mean to vary the matching difficulty. For that we used shape-context shape

1. <http://www.robots.ox.ac.uk/~vgg/data/data-aff.html>.

2. <http://vasc.ri.cmu.edu/idb/html/motion/hotel/index.html>.

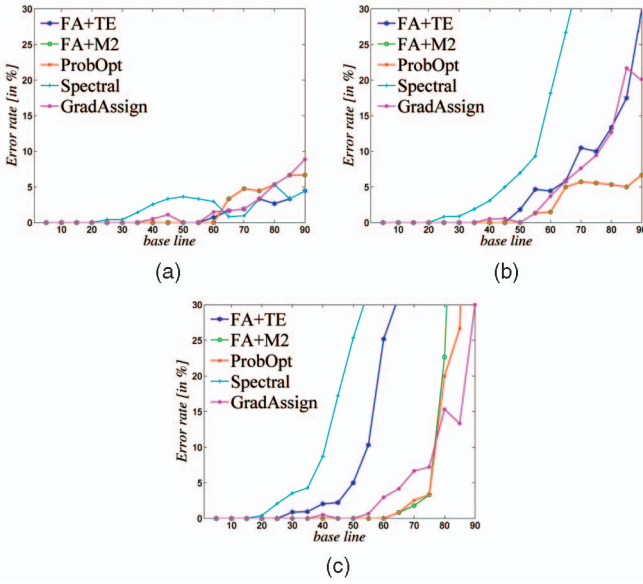


Fig. 16. *Hotel* series analysis results. We tracked 30 points using a varying number of  $K$  possible assignments. (a)  $n = 30, K = 10$ , (b)  $n = 30, K = 20$ , and (c)  $n = 30, K = 30$ .

descriptors [5] as a similarity measure between points. Hence, when matching a point in a particular frame, it can only be matched to its  $K$  nearest shape descriptors.

The results for the *Hotel* sequence are depicted in Fig. 16. It consists of 101 frames and 30 landmark points, where its motion is close to rigid and there are no significant scale changes or outliers. We vary  $K = \{10, 20, 30\}$ , where, for  $K = 10$ , the matching problem is well constrained and all schemes perform similarly. The decline in the accuracy for large baseline values is due to the inaccuracy of the shape descriptors as the deformation became substantial. Hence, the true matching might not be within the  $K = 10$  nearest neighbors of the SCs.

As  $K$  increases to  $\{20, 30\}$ , we witness the susceptibility of the pure spectral approaches (SM and FA+TE) to outliers as their accuracy deteriorates. As expected, the proposed dual marginalization-spectral scheme (FA+M2) outperformed the FA+TE, due to the numerical instability of the eigendecomposition of tensors.

We repeated the above experiment with the *House* sequences that consist of 30 landmark points and 111 frames. The motion in this sequence is more rigid than in the *Hotel* sequence and easier to match. This is confirmed by the results reported in Fig. 17. For  $K = 10$  all algorithms were able to match all of the points, while for  $K = 20$ , the SM is the first to fail, while for  $K = 30$ , the GA also fails by up to 10 percent.

#### 4.4 Implementation Issues

The proposed scheme was implemented in Matlab, where the construction of the affinity tensor was coded in a MEX file as it is loop-intensive. We used the Tensor Toolbox [4] to represent the sparse affinity tensors, and modified the HOPM solver within the Tensor Toolbox to efficiently handle symmetric tensors. For local features detectors and descriptors we used the open source Matlab implementation of Vedaldi and Fulkerson [39]. We also used the open source Matlab code of Timothee Cour<sup>3</sup> as a reference for

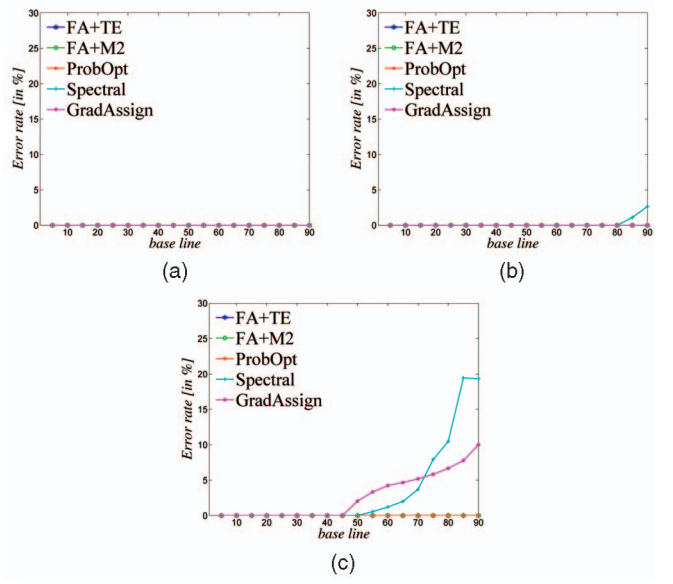


Fig. 17. *House* series analysis results. We tracked 30 points using a varying number of  $K$  possible assignments. (a)  $n = 30, K = 10$ , (b)  $n = 30, K = 20$ , and (c)  $n = 30, K = 30$ .

implementing the spectral matching and the Graduated Assignment algorithms. For the Probabilistic Graph Matching of Zass and Shashua, we used their publicly available Matlab code.<sup>4</sup>

On average, the memory space required for matching two images was 40 MB, needed for storing the sparse affinity tensor. It follows that, without the use of the random sparsification, this scheme would have been significantly less practical. It typically took a second to construct the affinity tensor and another two seconds to compute its ROA. The timings were taken on a computer running an Intel Core2 Duo processor at 2.2 GHz.

## 5 SUMMARY AND DISCUSSION

In this work, we presented a general framework for solving high order assignment problems. The high order affinities are encoded in an affinity tensor  $\Omega_m$ . It is based on the core assumption that the affinity measure  $\Omega_m$  encodes the joint assignment probabilities.  $\Omega_m$  is application specific and can be made invariant to certain deformations. We derived a marginalization scheme that maps a triplets tensor to matrix or a vector. By further assuming statistical independence among different assignments, we showed that the assignments can be recovered by the ROA of the affinity tensor/matrix. For tensors, we used the HOPM to recover the ROA, as spectral relaxation does not extend well to tensors. We also showed how to sparsify the affinity tensor during its construction, making the Tensor-HOA computationally feasible. The scheme was shown to be effective in registering sets of points as well as real images.

## REFERENCES

- [1] D. Achlioptas and F. Mcsherry, "Fast Computation of Low-Rank Matrix Approximations," *J. ACM*, vol. 54, no. 2, p. 9, 2007.
- [2] S. Agarwal, K. Branson, and S. Belongie, "Higher Order Learning with Graphs," *Proc. Int'l Conf. Machine Learning*, pp. 17-24, 2006.

3. <http://www.seas.upenn.edu/~timothee/>.

4. <http://www.cs.huji.ac.il/~zass/gm/>.

- [3] S. Agarwal, J. Lim, L. Zelnik-Manor, P. Perona, D. Kriegman, and S. Belongie, "Beyond Pairwise Clustering," *Proc. IEEE Conf. Computer Vision and Pattern Recognition*, vol. 2, pp. 838-845, 2005.
- [4] B.W. Bader and T.G. Kolda, "Matlab Tensor Toolbox Version 2.2," Jan. 2007.
- [5] S. Belongie, J. Malik, and J. Puzicha, "Shape Matching and Object Recognition Using Shape Contexts," *IEEE Trans. Pattern Analysis and Machine Intelligence*, vol. 24, no. 4, pp. 509-522, Apr. 2002.
- [6] A.C. Berg, T.L. Berg, and J. Malik, "Shape Matching and Object Recognition Using Low Distortion Correspondences," *Proc. IEEE Conf. Computer Vision and Pattern Recognition*, vol. 1, pp. 26-33, June 2005.
- [7] K.C. Chang, K. Pearson, and T. Zhang, "Perron-Frobenius Theorem for Nonnegative Tensors," *Comm. Math. Sciences*, vol. 6, no. 2, pp. 507-520, Dec. 2008.
- [8] F. Chung, "Spectral Graph Theory," *CBMS-AMS*, no. 92, Am. Math. Soc., May 1997.
- [9] D. Conte, P. Foggia, C. Sansone, and M. Vento, "Thirty Years of Graph Matching in Pattern Recognition," *Int'l J. Pattern Recognition and Artificial Intelligence*, vol. 18, no. 3, pp. 265-298, 2004.
- [10] T. Cour, P. Srinivasan, and J. Shi, "Balanced Graph Matching," *Advances in Neural Information Processing Systems 19*, B. Schölkopf, J. Platt, and T. Hoffman, eds., pp. 313-320, MIT Press, 2007.
- [11] O. Duchenne, F. Bach, I. Kweon, and J.J. Ponce, "A Tensor-Based Algorithm for High-Order Graph Matching," *Proc. IEEE Conf. Computer Vision and Pattern Recognition*, pp. 1980-1987, June 2009.
- [12] A. Egozi, Y. Keller, and H. Guterman, "A Probabilistic Approach to Spectral Graph Matching," *IEEE Trans. Pattern Analysis and Machine Intelligence*, to appear.
- [13] S. Gold and A. Rangarajan, "A Graduated Assignment Algorithm for Graph Matching," *IEEE Trans. Pattern Analysis and Machine Intelligence*, vol. 18, no. 4, pp. 377-388, Apr. 1996.
- [14] G.H. Golub and C.F. van Loan, *Matrix Computations*, third ed. Johns Hopkins Univ. Press, 1996.
- [15] V.M. Govindu, "A Tensor Decomposition for Geometric Grouping and Segmentation," *Proc. IEEE CS Conf. Computer Vision and Pattern Recognition*, vol. 1, pp. 1150-1157, 2005.
- [16] J.H. Hays, M. Leordeanu, A.A. Efros, and Y. Liu, "Discovering Texture Regularity via Higher-Order Matching," *Proc. Ninth European Conf. Computer Vision*, pp. 522-535, May 2006.
- [17] E. Kofidis and P.A. Regalia, "On the Best Rank-1 Approximation of Higher-Order Supersymmetric Tensors," *SIAM J. Matrix Analysis and Applications*, vol. 23, no. 3, pp. 863-884, 2001.
- [18] T.G. Kolda, "A Counterexample to the Possibility of an Extension of the Eckart-Young Low-Rank Approximation Theorem for the Orthogonal Rank Tensor Decomposition," *SIAM J. Matrix Analysis and Applications*, vol. 24, no. 3, pp. 762-767, Jan. 2003.
- [19] T.G. Kolda and B.W. Bader, "Tensor Decompositions and Applications," *SIAM Rev.*, vol. 51, no. 3, Sept. 2009.
- [20] L.D. Lathauwer, B.D. Moor, and J. Vandewalle, "A Multilinear Singular Value Decomposition," *SIAM J. Matrix Analysis and Applications*, vol. 21, no. 4, pp. 1253-1278, 2000.
- [21] L.D. Lathauwer, B.D. Moor, and J. Vandewalle, "On the Best Rank-1 and Rank-( $r_1, r_2, \dots, r_m$ ) Approximation of Higher-Order Tensors," *SIAM J. Matrix Analysis and Applications*, vol. 21, no. 4, pp. 1324-1342, 2000.
- [22] M. Leordeanu and M. Hebert, "A Spectral Technique for Correspondence Problems Using Pairwise Constraints," *Proc. IEEE Int'l Conf. of Computer Vision*, vol. 2, pp. 1482-1489, Oct. 2005.
- [23] E. Liberty, F. Woolfe, P.-G. Martinsson, V. Rokhlin, and M. Tygert, "Randomized Algorithms for the Low-Rank Approximation of Matrices," *Proc. Nat'l Academy of Sciences USA*, pp. 20167-20172, Dec. 2007.
- [24] L.-H. Lim, "Singular Values and Eigenvalues of Tensors: A Variational Approach," *Proc. First IEEE Int'l Workshop Computational Advances in Multi-Sensor Adaptive Processing*, pp. 129-132, Dec. 2005.
- [25] C.K. Liu, A. Hertzmann, and Z. Popović, "Learning Physics-Based Motion Style with Nonlinear Inverse Optimization," *ACM Trans. Graphics*, vol. 24, no. 3, pp. 1071-1081, Aug. 2005.
- [26] D. Lowe, "Distinctive Image Features from Scale Invariant Keypoints," *Int'l J. Computer Vision*, vol. 20, pp. 91-110, 2003.
- [27] J.A. Maciel and J.A.P. Costeira, "A Global Solution to Sparse Correspondence Problems," *IEEE Trans. Pattern Analysis and Machine Intelligence*, vol. 25, no. 2, pp. 187-199, Feb. 2003.
- [28] K. Mikolajczyk and C. Schmid, "A Performance Evaluation of Local Descriptors," *IEEE Trans. Pattern Analysis and Machine Intelligence*, vol. 27, no. 10, pp. 1615-1630, Oct. 2005.
- [29] K. Mikolajczyk, T. Tuytelaars, C. Schmid, A. Zisserman, J. Matas, F. Schaffalitzky, T. Kadir, and L. Van Gool, "A Comparison of Affine Region Detectors," *Int'l J. Computer Vision*, vol. 65, nos. 1/2, pp. 43-72, 2005.
- [30] H. Mirzaalian, G. Hamarneh, and T. Lee, "A Graph-Based Approach to Skin Mole Matching Incorporating Template-Normalized Coordinates," *Proc. IEEE Conf. Computer Vision and Pattern Recognition*, pp. 2152-2159, June 2009.
- [31] J. Munkres, "Algorithms for the Assignment and Transportation Problems," *J. SIAM*, vol. 5, no. 1, pp. 32-38, 1957.
- [32] J. Philbin and A. Zisserman, "The Oxford Buildings Data Set," <http://www.robots.ox.ac.uk/vgg/data/oxbuildings/index.html>, 2009.
- [33] C. Pierre, G. Golub, L.-H. Lim, and B. Mourrain, "Symmetric Tensors and Symmetric Tensor Rank," *SIAM J. Matrix Analysis and Applications*, vol. 30, no. 3, pp. 1254-1279, 2008.
- [34] T. Sarlos, "Improved Approximation Algorithms for Large Matrices via Random Projections," *Proc. 47th Ann. IEEE Symp. Foundations of Computer Science*, pp. 143-152, 2006.
- [35] G. Scott and H.L. Higgins, "An Algorithm for Associating the Features of Two Images," *Proc. Royal Soc. London*, vol. B-244, pp. 21-26, 1991.
- [36] A. Shashua, R. Zass, and T. Hazan, "Multi-Way Clustering Using Super-Symmetric Non-Negative Tensor Factorization," *Proc. European Conf. Computer Vision*, A. Leonardis, H. Bischof, and A. Pinz, eds., pp. 595-608, 2006.
- [37] J. Shi and J. Malik, "Normalized Cuts and Image Segmentation," *IEEE Trans. Pattern Analysis and Machine Intelligence*, vol. 22, no. 8, pp. 888-905, Aug. 2000.
- [38] L. Torresani, V. Kolmogorov, and C. Rother, "Feature Correspondence via Graph Matching: Models and Global Optimization," *Proc. 10th European Conf. Computer Vision*, pp. 596-609, 2008.
- [39] A. Vedaldi and B. Fulkerson, "VLFeat: An Open and Portable Library of Computer Vision Algorithms," <http://www.vlfeat.org/>, 2008.
- [40] R. Zass and A. Shashua, "Probabilistic Graph and Hypergraph Matching," *Proc. IEEE Conf. Computer Vision and Pattern Recognition*, pp. 1-8, June 2008.
- [41] D. Zhou, J. Huang, and B. Schölkopf, "Learning with Hypergraphs: Clustering, Classification, and Embedding," *Advances in Neural Information Processing Systems 19*, B. Schölkopf, J. Platt, and T. Hoffman, eds., pp. 1601-1608, MIT Press, 2007.



**Michael Chertok** received the BSc degree in computer engineering from the Technion-Israel Institute of Technology, Haifa, in 1998. He is currently pursuing a PhD degree in electrical engineering at Bar-Ilan University, Israel. He has vast industry experience in computer vision and image processing. His research interests include data analysis using graphs, video compression and analysis, and optimization.



**Yosi Keller** received the BSc degree in electrical engineering from the Technion-Israel Institute of Technology, Haifa, in 1994, and the MSc and PhD degrees in electrical engineering from Tel-Aviv University, Israel, in 1998 and 2003, respectively. From 1994 to 1998, he was an R&D officer in the Israeli Intelligence Force. From 2003 to 2006, he was a Gibbs Assistant Professor with the Department of Mathematics, Yale University. He is a senior lecturer in the

Electrical Engineering Department at Bar Ilan University, Israel. His research interests include graph-based data analysis, optimization, and spectral graph theory-based dimensionality reduction.

► For more information on this or any other computing topic, please visit our Digital Library at [www.computer.org/publications/dlib](http://www.computer.org/publications/dlib).